Hypersonic Viscous Flows Past General Bodies at Angle of Attack and Yaw

M.D. Kim* and C.H. Lewis†
Virginia Polytechnic Institute and State University, Blacksburg, Virginia

Computational results of hypersonic viscous flows over blunt-nosed complex re-entry bodies are presented. An implicit iterative numerical scheme at each marching step is used to solve the parabolized Navier-Stokes (PNS) equations. An existing PNS code has been extended to treat nonaxisymmetric bodies at angle of attack and yaw, multiconic bodies with spin, surface mass transfer, and adiabatic wall conditions. Boundary conditions take into account the periodic condition around the body due to the yaw or spin, and the mass-transfer and/or spin effects at the body surface. The computational results presented include surface-measurable quantities and aerodynamic force and moment coefficients for complex geometries; available data were used for comparison. Grid-size effects on the accuracy of the Magnus force components due to spin are also discussed.

Nomenclature

CA	= axial force coefficient
CFS	= streamwise skin-friction coefficient, $2\tau_s^*/(\rho_\infty U_\infty^2)$
CFW	= cross flow skin-friction coefficient, $2\tau_\phi^*/(\rho_\infty U_\infty^2)$
C_m	= pitching moment coefficient about blunt nosetip
C_n	= Magnus moment coefficient about blunt nosetip
CN	= normal force coefficient
c_p	= constant pressure specific heat
CY	= side force coefficient
$CY1$	= component of Magnus force due to streamwise shear
$CY2$	= component of Magnus force due to surface pressure
$CY3$	= component of Magnus force due to transverse shear
g	= determinant of coordinate metric tensor
g_{ij}	= coordinate metric tensor, $i,j=1,2,3$
g_1,g_2,g_3	= vectors in ξ_1,ξ_2,ξ_3 coordinate system
h	= static enthalpy, $h^*/(c_p^* T_\infty)$
H	= total enthalpy, H^*/U_∞^2
$\boldsymbol{i,j,k}$	= unit vectors in x,y,z body axis
$\dot{m}$	= mass-transfer rate at wall, $\rho_w^* v_w^*/\rho_\infty U_\infty$
M	= freestream Mach number
NSH	= shock stand-off distance divided by R_n
p	= nondimensional pressure, $p^*/(\rho_\infty U_\infty^2)$
PHI	= angular coordinate around body, ϕ
$PWALL$	= nondimensional wall pressure, $p_w^*/(\rho_\infty U_\infty^2)$
Pr	= Prandtl number
q	= heat-transfer rate, $q^*/(\rho_\infty U_\infty^3)$
Re_∞/ft	= freestream unit Reynolds number
R_n	= dimensional body nose radius of curvature
s	= surface distance measured along body
S/RN	= surface distance measured along body, s^*/R_n
$STINF$	= Stanton number, $q^*/[\rho_\infty U_\infty (H_0^* - H_w^*)]$
T	= temperature, T^*/T_∞
T_0	= freestream stagnation temperature
T_{ref}	= reference temperature, $(\gamma-1)M^2 T_\infty$ or U_∞^2/c_p^*
T_w	= wall temperature, T_w^*/T_∞
U_∞	= dimensional freestream velocity
u,v,w	= velocity tensors in computational coordinates
V	= velocity vector of fluid flow
x,y,z	= body axes with x leeward, y downward
X_{cp}	= location of center of pressure from blunt nosetip
z,r,ϕ	= body-oriented cylindrical coordinates
α	= angle of attack, deg
β	= angle of yaw, deg
γ	= ratio of specific heats
ϵ	= perturbation parameter, $\epsilon^2 = \mu^*(T_{ref})/(\rho_\infty U_\infty R_n)$
θ_c	= cone half-angle, deg
μ	= coefficient of viscosity, μ^*/μ_∞
ρ	= density, ρ^*/ρ_∞
τ_s	= primary flow wall shear stress, $\tau_s^*/(\rho_\infty U_\infty^2)$
τ_ϕ	= cross-flow wall shear stress, $\tau_\phi^*/(\rho_\infty U_\infty^2)$
ω	= angular velocity, rps
ξ_1,ξ_2,ξ_3	= body-normal shock-normal computational coordinates

Superscript

*	= dimensional quantity

Subscripts

w	= wall value
0	= stagnation condition
∞	= freestream condition (dimensional quantity)

Introduction

IN recent years, active development of computational methods using parabolized Navier-Stokes (PNS) equations has been accomplished by many investigators. For instance, Helliwell et al.[1] developed the HYTAC code using a typical PNS approach and employing a general body-normal shock-normal coordinate system. The HYTAC method was developed based on a previous PNS method called LUB1,[2] which can be used only for a conical body. The PNS methods can solve the entire re-entry flowfield including the cross-flow separated region using an efficient marching scheme along the body, provided streamwise flow separation does not occur. Computational results are accurate in most cases when enough grid points are used and proper initial plane data are

Received Jan. 22, 1982; revision received Sept. 28, 1982.

*Graduate Student, Aerospace and Ocean Engineering Department. Student Member AIAA.

†Professor. Associate Fellow AIAA.

supplied. The range of applicability covers supersonic and hypersonic, laminar-transitional-turbulent, and perfect or equilibrium gas flows. Computation time is also reasonable and some examples will be presented later.

Spin effects on the hypersonic viscous flowfield past conical bodies have previously been analyzed by Agarwal and Rakich.[3] They discussed effects of flow parameters on the direction of the Magnus force components. Complex coupling effects of mass transfer and/or spin on the surface-measurable quantities and Magnus force components were analyzed for a sphere-cone by Kim and Lewis,[4] but those studies were based on the LUB1 method whose application was restricted to conical bodies.

The main purpose of this paper is to modify the HYTAC code in order to extend its applicability to treat a complex nonaxisymmetric body at angle of attack and yaw. Further extension has been accomplished for the case of a complex body with spinning motion, mass transfer, and/or adiabatic wall. Computational results for various geometries are presented together with comparisons of available data. An analysis of grid-size effect on the direction of Magnus force components is also presented.

In the following sections, theoretical background and numerical procedure are presented followed by the results. Basic theories for the modification to include yaw and spin will be presented. A brief overview of the governing equations, coordinate system, and numerical procedure will be given. A discussion of the boundary conditions for mass transfer or adiabatic wall is also included.

Analysis

Coordinate System

The definition of a coordinate system is one of the most important steps in building a numerical technique for a fluid-flow analysis. The computational grid will be distributed along the constructed coordinate lines. In the present study, a body-oriented, nonorthogonal coordinate system (ξ_1,ξ_2,ξ_3) was constructed to have the following characteristics:

1) The body is a coordinate surface ($\xi_2=0$).
2) The ξ_1 and ξ_3 coordinates are necessarily orthogonal only at the body.
3) The ξ_2 coordinate is always orthogonal to ξ_1 and ξ_3.
4) The bow shock is an ξ_1,ξ_3 coordinate surface.

Figure 1 shows the body-oriented computational coordinate system. This coordinate system is appropriate to obtain a solution for a complex geometry that has body surface slope discontinuities. The HYTAC code determines a proper streamwise marching stepsize, considering the number of iterations taken for the previous solution, and at the new streamwise station the code constructs ξ_1,ξ_3 coordinate lines.

The third-coordinate lines (ξ_3) are constructed to be normal to the ξ_1 coordinate on the body surface. An orthogonal grid on the body surface makes it easier to integrate forces and moments and also to include various wall boundary conditions. The second coordinate (ξ_2) is constructed to be normal to both ξ_1 and ξ_3 coordinate lines in the region between the body and the shock surface. Since the shock surface is taken as an ξ_1,ξ_3 coordinate surface, the resulting ξ_2 coordinate lines become both body-normal and shock-normal. In this coordinate system, the application of the shock boundary condition becomes simple, because the ξ_2 coordinate is normal to the shock surface.

The reference coordinate system for the interpretation of body geometry, shock shape, and every computational grid point is a body-oriented cylindrical coordinate system; that is,

$$\xi_1=\xi_1(z,r,\phi)$$

$$\xi_2=\xi_2(z,r,\phi)$$

$$\xi_3=\xi_3(z,r,\phi)$$

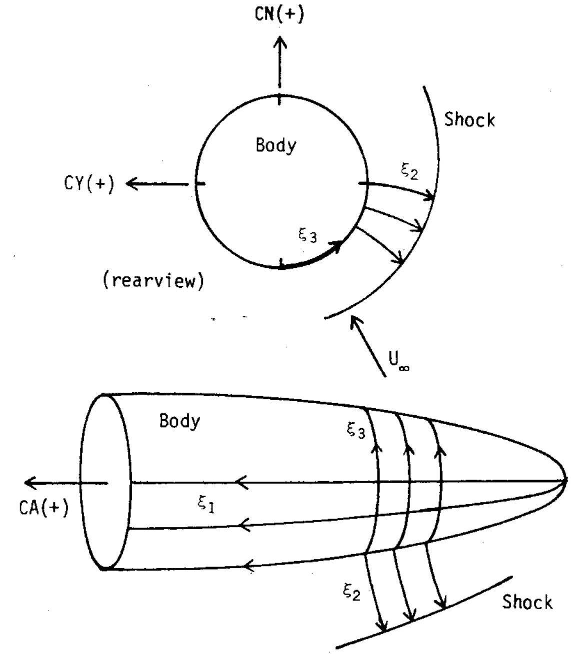

Fig. 1 Surface-oriented coordinate system.

When the computational grids are constructed in this manner, generally the ξ_1 and ξ_3 coordinates will not be orthogonal to each other in the region between the body and the shock. Hence the coordinate metric tensor g_{ij}, which is related to the nonorthogonality and coordinate stretching, will appear in the governing equations. In addition, the determinant of the metric g becomes an important factor in the governing equations. The complete procedure to generate coordinates is given by Helliwell et al.[1]

Governing Equations

The governing equations for the present study are based on the steady parabolized Navier-Stokes equations first derived for a conical body by Lubard and Helliwell.[2] In a general curvilinear coordinate system, the steady parabolized Navier-Stokes equations are written in nondimensionalized form with the velocity vector written as

$$V=ug_1+vg_2+wg_3$$

where u, v, and w are tensor velocity components. The physical components are obtained by multiplying the respective term by its metric factor.

In the equations for the stress tensor components, all derivatives with respect to the streamwise direction were neglected. The resulting equations are parabolic in the streamwise direction and elliptic in the other directions. The flow variables are nondimensionalized by their freestream values. The entire flow regime of laminar, transitional, and turbulent has been considered. In addition, an equilibrium real gas option was also included. The complete set of the governing equations is given by Helliwell et al.[1]

Alpha and Yaw

The HYTAC code has been extended for the analysis of a nonaxisymmetric body at angle of attack and yaw. In this case the flowfield is no longer symmetric about the plane of symmetry of the body. Therefore, the flowfield must be solved for the entire surface around the body using a periodic boundary condition. The yaw angle is the angle between the plane of symmetry of the body and the plane containing actual wind vector and a line in the plane of symmetry that is orthogonal to the zero angle of attack, zero yaw wind vector (i.e., i vector of body axes). In both the Cartesian and the computational coordinates, the freestream flow velocity is given by

$$V_\infty = \cos\alpha\sin\beta i - \sin\alpha j - \cos\alpha\sin\beta k$$
$$= u_\infty g_1 + v_\infty g_2 + w_\infty g_3$$

where, in the body axes, i is backward, j is downward of body, and k is to the right in a rear view. The transformation matrix taken from i,j,k into the local computational coordinates g_1, g_2, g_3 gives u_∞, v_∞, w_∞ in terms of α and β.

Boundary Conditions

The following conditions are used for the boundary conditions at body surface with mass transfer and spin.

u = 0 (no slip)
v = specified distribution for mass transfer
w = specified distribution for spin
h = specified distribution or adiabatic wall

$$\left[\frac{\partial p}{\partial \xi_2}\right]_w = -\frac{g_{22}}{g^{1/2}}\left[\frac{\partial}{\partial \xi_2}(\rho v^2 g^{1/2}) + \frac{\partial}{\partial \xi_3}(\rho v w g^{1/2})\right]$$
$$+\frac{1}{Re_\infty}\left[\frac{4}{3}\left(\frac{\partial \mu}{\partial \xi_2}\frac{\partial v}{\partial \xi_2} + \mu\frac{\partial^2 v}{\partial \xi_2^2}\right)\right.$$
$$+\frac{g_{11}g_{22}}{g}\left(\frac{\partial \mu}{\partial \xi_3}\frac{\partial v}{\partial \xi_3} + \mu\frac{\partial^2 v}{\partial \xi_3^2}\right)$$
$$\left.+\left(\frac{\partial \mu}{\partial \xi_3}\frac{\partial w}{\partial \xi_2} + \frac{\mu}{3}\frac{\partial^2 w}{\partial \xi_2 \partial \xi_3}\right)\right]$$

We have two options to obtain wall pressure for the mass-transfer and spin case. One is to use the continuity equation, and the other considers the v-momentum equation. By numerical experiments it has been found that the latter gave more stable solutions while the former rarely produced a converged solution. Thus, for the present analysis the v-momentum equation has been used and it was differenced using a one-sided difference scheme to provide the pressure at body boundary.

In order to obtain the outer boundary conditions, Rankine-Hugoniot jump conditions are utilized at the shock. From freestream components and jump conditions, five conservation equations are obtained, which can be used to determine the aftershock properties. To determine the shock stand-off distance, one more equation is required. Thus one-sided differencing of the continuity equation provides the sixth equation.

Since the windward and leeward surfaces are not symmetry planes for general bodies with spin or yaw, a periodic condition for the flow profiles around the body is specified in the windward plane, thus providing boundary conditions in the ξ_3 direction.

The adiabatic wall option has been included by using the condition $(dh/d\xi_2)_w = 0$. Assuming very small stepsizes in body-normal direction near the wall, this condition is written in the code as $h(1,L) = h(2,L)$.

Initial Conditions

For a numerical flowfield solution which utilizes a marching scheme, preparation of an accurate initial data plane (IDP) is one of the most crucial conditions for the successful start of a downstream solution. By previous investigations,[5,6] the viscous shock-layer method (VSL3D)[7] for blunt bodies was found to be able to generate satisfactory initial plane data to start the PNS solution. Thus, the entire flow properties, including a shock shape, must be supplied at the initial data plane to start the HYTAC code.

In the present work, a streamwise station on the sphere nose is chosen, and at the station a body-normal shock-normal IDP for HYTAC is constructed by proper interpolations and rotations of the VSL3D solution. By numerical experiment it has been found that the starting station should be between the sonic point and the sphere-cone juncture, but it should be well forward from the sphere-cone juncture for a successful start. In the preparation of the IDP for the test cases, the spherical nosetips of the bodies were considered to have neither spin nor mass transfer.

Numerical Solution

The equations are solved by implicit differencing in the ξ_2,ξ_3 plane. The ξ_1 derivatives are approximated by a backward difference while ξ_2 and ξ_3 derivatives use an unequally spaced three-point-difference formula. The PNS equations and the perturbation equations during the iterations can be written in the matrix form:

$$F(U) = 0, \qquad \Delta^n = U^{n+1} - U^n$$

where F denotes the governing equations for the unknowns U, and Δ^n is the column matrix of perturbation properties at the nth iteration.

After differencing, the equations are linearized by the Newton-Raphson method. Thus, all the nonlinear terms of perturbation properties are dropped. This results in an equation of the form

$$M(U^n)\Delta^n = -F(U^n) \qquad n = 0,1,2,\ldots$$

with U^0 an initial guess to the solution of the governing equations, and M the Jacobian of F. Because of the size of the system, instead of solving the above equation directly, the Gauss-Seidel iteration method is used. In the ξ_3 direction, an implicit-iterative scheme[1] is used, but after convergence, the solution obtained is a fully implicit one. After convergence, another step in the marching direction is taken and the whole procedure is repeated.

The marching stepsize is controlled internally by the code, considering the number of iterations taken for the solution at the previous step. Careful stepsize control is very important in order to obtain a solution when large disturbances exist due to body slope change, mass transfer, cross-flow separation, and/or high wall temperature.

Results and Discussion

As discussed previously, an existing PNS code was extended to treat more general cases, and computational results of hypersonic viscous flow over blunt-nosed complex re-entry bodies have been obtained. Boundary conditions were ex-

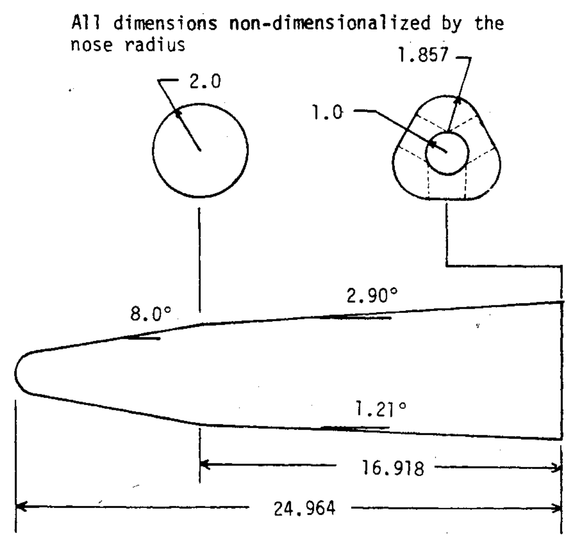

Fig. 2 Geometry of sphere-cone-triangle (case 1).

Table 1 Test case conditions

Case	Altitude, s/R_n	Mach, R_n(m)	Re_∞/m, θ_c(deg)	U_∞(m/s), α (deg)	T_∞(K) β(deg)	T_w(K) ω(rps)	T_w/T_0, $\dot{m}$	ϵ
1[a]	61.0 km	22.95	1.247E5	7315.0	253.0	1012.	0.0376	0.050
	24.2	0.0686	8.0	8.65	5.04	0.0	0.0	
2[b]	W-T	4.00	9.220E6	1277.0	253.6	255.6	0.24	0.0066
	30.0	0.0085	10.0	2.0	0.0	500.	0.0	
3[c]	30.5 km	25.0	8.626E6	7571.0	228.3	3000.	0.1043	0.0103
	30.8	0.0254	16.0	2.0	0.0	1000.	0.0	

[a]Sphere-cone-triangle. [b]Sphere-cone. [c]Sphere-cone-cylinder-flare.

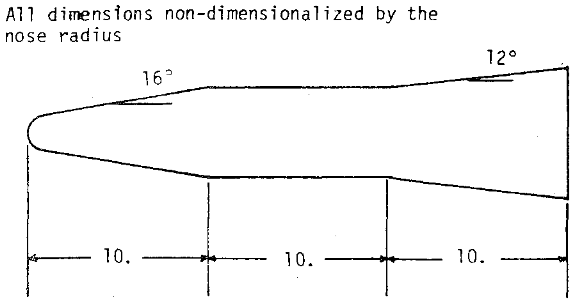

Fig. 3 Geometry of sphere-cone-cylinder-flare (case 3).

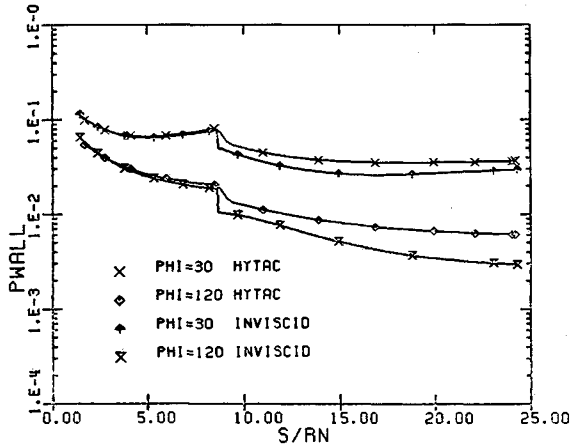

Fig. 4 Case 1, surface pressure distribution along the body.

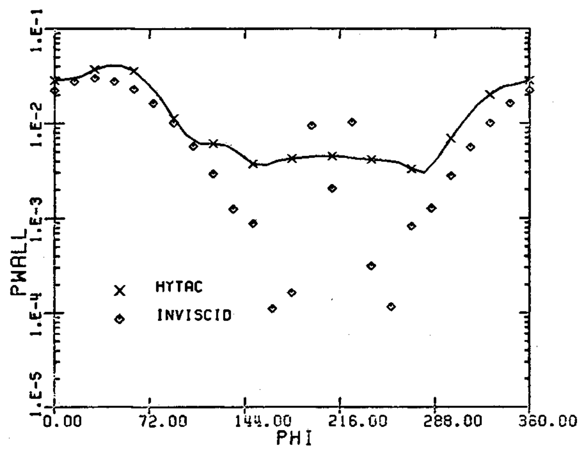

Fig. 5 Case 1, surface pressure distribution around the body at $s/Rn = 24.2$.

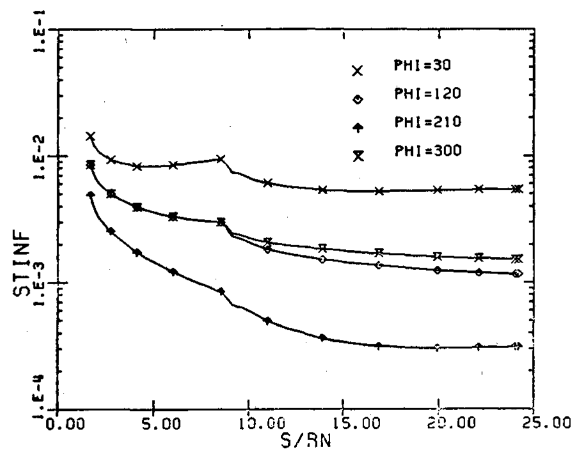

Fig. 6 Case 1, surface heat-transfer distribution along the body.

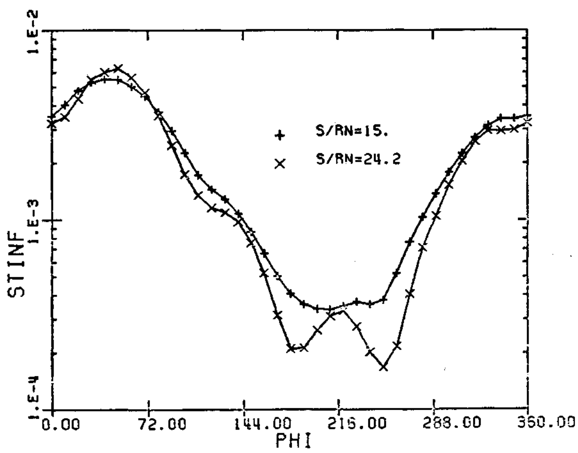

Fig. 7 Case 1, surface heat-transfer distribution around the body.

tended to take into account the periodic condition around the body due to yaw or spin, and the effects of mass transfer and/or spin at the body surface. To test the validity of the present method, three test cases were chosen and the results obtained were compared with available data and discussed. Elsewhere[8] two additional test cases were considered. One was a sphere-cone whose results compared well with the experimental data given by Kinslow[9] and Boylan.[10] The other case was a sphere-cone with surface mass transfer, and the results were compared with the PNS solution obtained by the LUB1 code. A summary of freestream conditions for the test cases considered in the present paper is given in Table 1 and the geometries are shown in Figs. 2 and 3.

The sample test case chosen for case 1 is a sphere-cone-triangular body at angle of attack and yaw, and the freestream conditions are given in Table 1. An 8.65-deg angle of attack and a 5.04-deg yaw correspond to the conditions of a bank angle of 30 deg and a resultant angle of attack of 10 deg. Figure 4 shows the wall pressure distribution along the body. The inviscid solution obtained by the CM3DT[11] and 3IS[12] codes agrees well over the conical body section. Downstream of the body axial slope discontinuity, the inviscid solution produced some amount of overexpansion when compared to the viscous solution. The present viscous solution shows relatively smooth turning over the discontinuity. The pressure distribution around the body at the body-end station is presented in Fig. 5. The curves show a complex cross flow turning phenomena over the triangular shaped body at angle of attack and yaw. The inviscid solution shows a severe overexpansion over the corners and then shows an inviscid pressure recovery. Figures 6 and 7 present surface heat-transfer distributions both along and around the body. The curve around the body clearly shows the effect of cross-flow separation at the body-end station.

The purpose of case 2 is to investigate the grid-size effect on the Magnus forces exerted on a spinning body at angle of attack. A sphere-cone at a 2-deg angle of attack with spin rate of 500 rps at Mach 4 is considered. Freestream parameters and body information are given in Table 1. This case is the one that has been analyzed by previous investigators,[3,13] reporting different directions of Magnus force components. There are three major components of Magnus force coefficient as shown in Fig. 8. *CY1* is the Magnus force component due to the integrated streamwise skin friction, *CY2* is due to the wall pressure distribution, and *CY3* is due to the transverse skin friction. In most cases, the *CY2* component

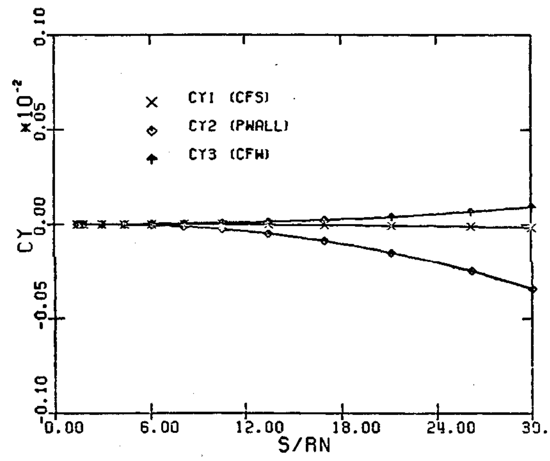

Fig 8 Case 2, Magnus force components distribution along the body.

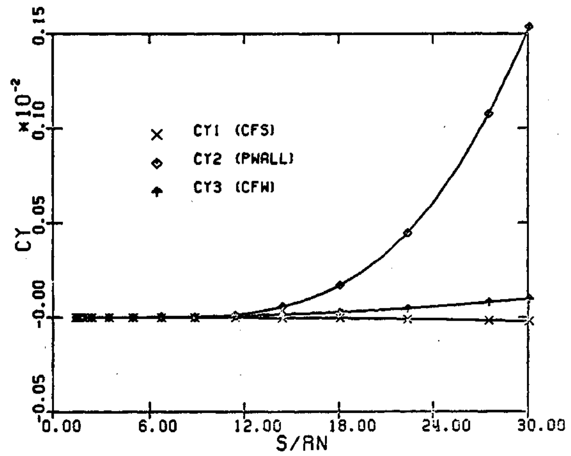

Fig. 9 Case 2, Magnus force components distribution along the body obtained by using a reduced body-normal grid size.

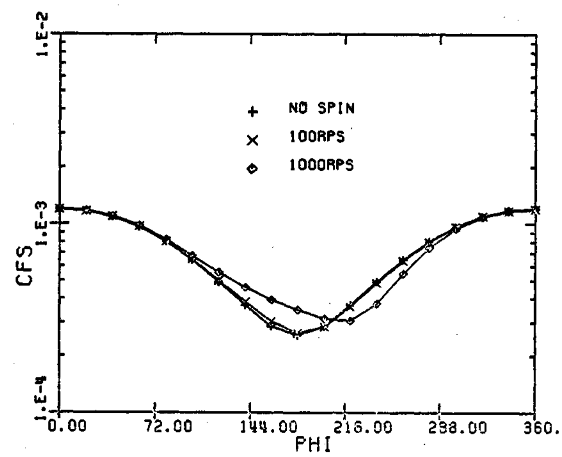

Fig. 10 Case 3, streamwise skin-friction distribution around the body at $s/Rn = 30.8$.

Table 2 Aerodynamic coefficients for test cases

Case	Method	CA	CN	CY	C_m	C_n	X_{cp}
1	HYTAC	0.2487	0.2394	0.1382	−0.1203	0.0695	0.5025
1	INVISCID (CM3DT + 3IS)	0.2034	0.2362	0.1405	−0.1030	0.0604	0.4340
2	HYTAC (101-19)	0.1780	0.0609	−0.00060	−0.0383	−0.00041	0.6293
2	HYTAC (50-19)	0.1776	0.0603	−0.00022	−0.0379	−0.00023	0.6281
3	HYTAC (1000 rps)	0.1105	0.0598	−0.00021	−0.0369	−0.00015	0.6169

Table 3 Computing times[a] for test cases

Case	Method	s/Rn	Grid size of s-Steps	Grid size of n-Points	Grid size of ϕ-Planes	Time (min)
1	HYTAC	24.2	87	50	37	126.15
1	INVISCID	24.2	175	15	25	18.23[b]
2	HYTAC	30.0	45	101	37	81.23
2	HYTAC	30.0	36	101	19	46.18
2	HYTAC	30.0	36	50	19	22.51
3	HYTAC	30.8	92	50	19	51.93

[a] CPU time on IBM 370/3032, H = OPT2 compiler. [b] 16.11 min for nose (CM3DT), 2.12 min for afterbody (3IS).

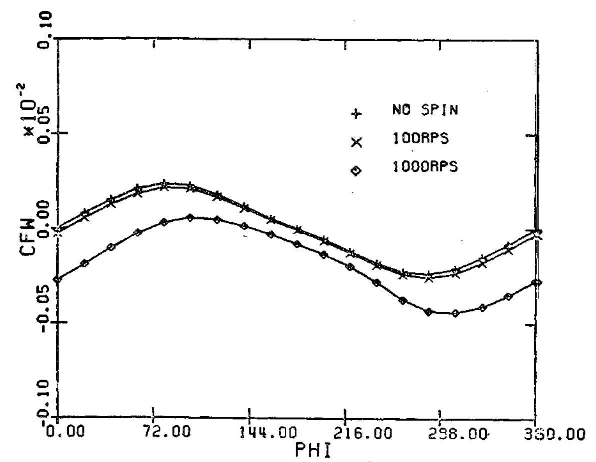

Fig. 11 Case 3, transverse skin-friction distribution around the body at $s/Rn = 30.8$.

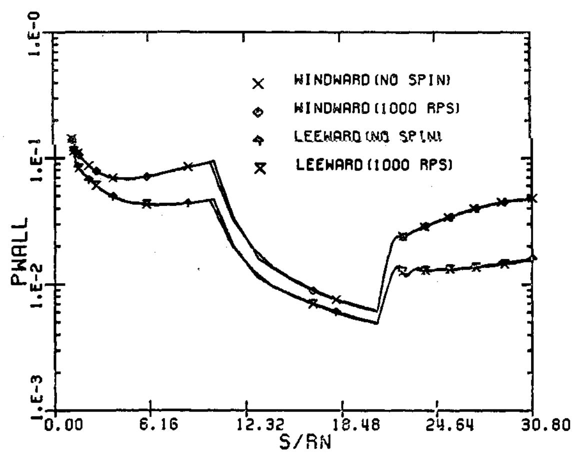

Fig. 12 Case 3, surface pressure distribution along the body.

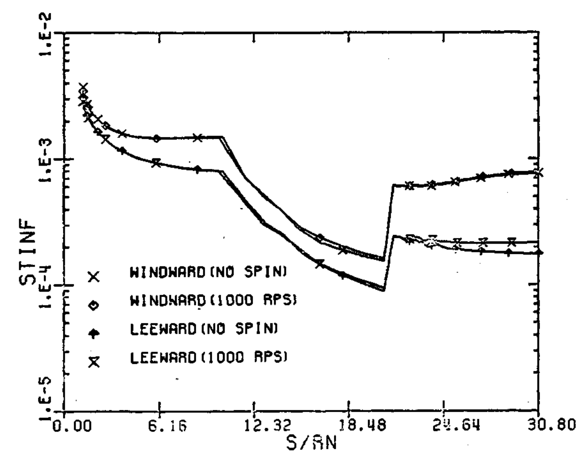

Fig. 13 Case 3, surface heat-transfer distribution alogn the body.

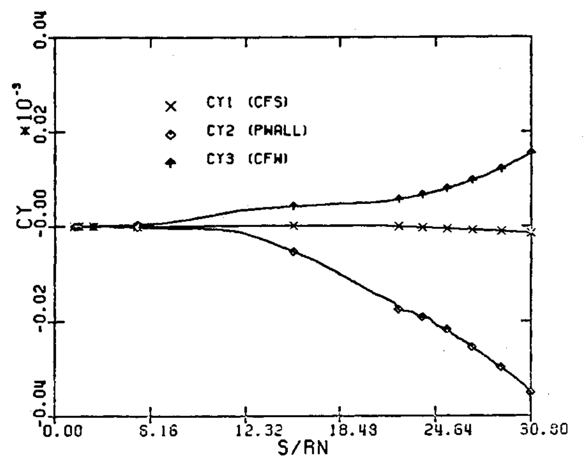

Fig. 14 Case 3, Magnus force components distribution along the body.

was dominant in comparison to other components. Figure 8 shows typical trends of the three Magnus components, where 101 grid points in the body-normal direction and 37 planes around the body were used. When 19 planes were used around the body, keeping 101 points in normal direction, the results were almost the same as before. However, when the normal grid was reduced to 50 points with 19 planes around the body, the *CY2* component changed its sign and increased in the positive direction as shown in Fig. 9; this is an erroneous result. This positive trend of *CY2* is similar to the result that has been reported in Ref. 3. From these results, it is observed that proper normal grid size is very important in order to obtain a physically meaningful solution for the Magnus force.

In case 3, a sphere-cone-cylinder-flare body with spin has been chosen, and various surface properties as well as the Magnus force coefficient were obtained. Each part of the cone, cylinder, and flare was about 10 nose-radii axial length, and the cone half angle is 16 deg and the flare angle is 12 deg. A freestream flow at Mach 25 and Re_∞/m 8.63×10^6 with a 2-deg angle of attack was considered. Results were obtained for three different spin rate options, i.e., no-spin, 100 rps, and 1000 rps. The effect of spin on the streamwise skin friction around the body is shown in Fig. 10. Noticeable spin effect appears only on the leeward side of the flare section. Figure 11 presents well distributed spin effect on the asymmetric transverse skin friction around the body. The surface pressure is not affected much by spin as shown in Fig. 12, while surface heat transfer is slightly affected in the downstream flare section as shown in Fig. 13. Figure 14 shows Magnus force component distributions along the body for case 3.

Summarized aerodynamic coefficients for the test cases are presented in Table 2. The reference area for the coefficients is the body base area, and the reference length is total body length. For case 1, the HYTAC result gives a higher axial force than the inviscid 3IS result due to viscous effects. The results for case 2 show that normal grid-size effect on the normal and axial forces is negligibly small, while the effect on the Magnus forces is very large.

Computing times based on an IBM 370/3032, H = OPT2 compiler are presented for the test cases in Table 3. Typical computing time for a sphere-cone at angle of attack is 10 min. The triangular body (case 1) had 37 planes around the body and complex body surface slope changes; accordingly, a large amount of computing time was required. The time comparisons for case 2 clearly show the grid-size effects on computing time in the HYTAC method.

Concluding Remarks

An existing PNS code was extended to treat more general cases, and computational results of hypersonic viscous flows over blunt-nosed complex re-entry bodies have been presented. Boundary conditions were extended to take into account the periodic condition around the body due to yaw or spin and the effect of mass transfer and/or spin at the body surface. The main results of the present study are summarized as follows:

1) The HYTAC code has been extended to treat nonaxisymmetric bodies at angle of attack and yaw, multiconic bodies with spin, surface mass transfer, and adiabatic wall conditions.

2) It was found that the accuracy and direction of Magnus force components due to spin are very sensitive to the variation of normal grid size.

3) *Computational results were presented for surface-measurable quantities and forces and moments of a triangular-shaped body at angle of attack and yaw.* The results of the present study compared well with available data.

References

[1] Helliwell, W.S., Dickinson, R.P., and Lubard, S.C., "HYTAC Phase I Report: Viscous Flow over Arbitrary Geometries at High Angle of Attack," Arete Associates Technical Report AR-79-046-TR, April 24, 1979.

[2] Lubard, S.C. and Helliwell, W.S., "Calculation of the Flow on a Cone at High Angle of Attack," *AIAA Journal*, Vol. 12, July 1974, pp. 965-974.

[3] Agarwal, R. and Rakich, J.V., "Computation of Hypersonic Laminar Viscous Flow Past Spinning Sharp and Blunt Cones at High Angle of Attack," AIAA Paper 78-65, Jan. 1978.

[4] Kim, M.D. and Lewis, C.H., "Computation of Hypersonic Laminar Viscous Flow over a Body with Mass Transfer and/or Spin," AIAA Paper 81-1044, June 1981.

[5] Waskiewicz, J.D. and Lewis, C.H., "Hypersonic Viscous Flows over Sphere-Cones at High Angles of Attack," *AIAA Journal*, Vol. 17, Feb. 1979, pp. 131-132.

[6] Gogineni, P.R. and Lewis, C.H., "Three-Dimensional Viscous Hypersonic Flows over General Bodies," AIAA Paper 80-0029, Jan. 1980.

[7] Murray, A.L. and Lewis, C.H., "Hypersonic Three-Dimensional Viscous Shock-Layer Flows over Blunt Bodies," *AIAA Journal*, Vol. 16, Dec. 1978, pp. 1279-1286.

[8] Kim, M.D. and Lewis, C.H., "Computation of Hypersonic Viscous Flow Past General Bodies at Angle-of-Attack and Yaw," AIAA Paper 82-0225, Jan. 1982.

[9] Kinslow, M., "Static Pressure on Sharp and Blunt Cones in Conical and Parallel Low-Density Flow," AEDC-TR-74-30, Nov. 1974.

[10] Boylan, D.E., "Laminar Heat Transfer on Sharp and Blunt Ten-Degree Cones in Conical and Parallel Low-Density Flow," AEDC-TR-73-106, Aug. 1973.

[11] Hall, D. and Dougherty, C., "Performance Technology Program (PTP-S II), Volume III—Inviscid Aerodynamic Predictions for Ballistic Re-entry Vehicles with Ablated Nosetips," Science Applications, Inc., Valley Forge, Pa., SAI-79-506-VF, Sept. 1979.

[12] Daywitt, J., Brant, D., and Bosworth, F., "Computational Technique for Three-Dimensional Inviscid Flow Fields about Re-entry Vehicles, Volume I—Numerical Analysis," SAMSO TR-79-5, April 1978.

[13] Sturek, W.B. and Schiff, L.B., "Computations of the Magnus Effect for Slender Bodies in Supersonic Flow," AIAA Paper 80-1586, 1980.